Biometals (2013) 26:693–703
DOI 10.1007/s10534-013-9641-3

Cobalt binding in the photosynthetic bacterium *R. sphaeroides* by X-ray absorption spectroscopy

Benny D. Belviso · Francesca Italiano · Rocco Caliandro · Benedetta Carrozzini · Alessandra Costanza · Massimo Trotta

Received: 3 April 2013 / Accepted: 2 June 2013 / Published online: 9 June 2013

Abstract Cobalt is an important oligoelement required for bacteria; if present in high concentration, exhibits toxic effects that, depending on the microorganism under investigation, may even result in growth inhibition. The photosynthetic bacterium *Rhodobacter* (*R.*) *sphaeroides* tolerates high cobalt concentration and bioaccumulates Co^{2+} ion, mostly on the cellular surface. Very little is known on the chemical fate of the bioaccumulated cobalt, thus an X-ray absorption spectroscopy investigation was conducted on *R. sphaeroides* cells to gain structural insights into the Co^{2+} binding to cellular components. X-ray absorption near-edge spectroscopy and extended X-ray absorption fine structure measurements were performed on *R. sphaeroides* samples containing whole cells and cell-free fractions obtained from cultures exposed to 5 mM Co^{2+}. An octahedral coordination geometry was found for the cobalt ion, with six oxygen-ligand atoms in the first shell. In the soluble portion of the cell, cobalt was found bound to carboxylate groups, while a mixed pattern containing equivalent amount of two sulfur and two carbon atoms was found in the cell envelope fraction, suggesting the presence of carboxylate and sulfonate metal-binding functional groups, the latter arising from sulfolipids of the cell envelope.

Keywords Cobalt coordination · Membrane · Sulfolipids · *Rhodobacter sphaeroides* · EXAFS

B. D. Belviso · R. Caliandro · B. Carrozzini
Istituto di Cristallografia, Consiglio Nazionale delle Ricerche, Via Amendola 122/O, 70126 Bari, Italy

F. Italiano (✉) · M. Trotta
Istituto per i Processi Chimico Fisici, Consiglio Nazionale delle Ricerche, Via Orabona 4, 70126 Bari, Italy
e-mail: f.italiano@ba.ipcf.cnr.it

A. Costanza
Dipartimento di Biologia, Università Aldo Moro di Bari, Via Orabona 4, 70126 Bari, Italy

Introduction

The increasing anthropogenic release of heavy metals in the environment raises strong concerns in the public opinion. Concerns are largely justified since heavy metal ions are harmful to health and may enter in the human metabolism *via* food chain (Albering et al. 1999; Forstner and Wittmann 1983; Nevin 2000). Among heavy metals, cobalt belongs to the class of oligonutrients for living organisms, together with nickel, copper, iron and few others. It is involved in various metabolic functions (Okamoto and Eltis 2011). Cobalt is an essential cofactor in vitamin B12-dependent enzymes and in few other proteins (Kobayashi and Shimizu 1999). It has a low abundance in natural environments, but mining and smelting activities, as well as industrial wastes, may lead to high cobalt contamination. At high concentration, cobalt is toxic to living cells: it increases the oxidative

stress by catalyzing the generation of reactive oxygen species (Kasprzak 1991; Leonard et al. 1998; Gault et al. 2010), it competes with other essential metal ions (i.e. Fe^{2+}, Mg^{2+}, Ca^{2+}), and may hinder correct macromolecular functions, modifying the ion transport (Giotta et al. 2007, 2008) and the enzyme structure (Jennette 1981) or binding to the sulfhydryl groups of some sensitive enzymes (Bruins et al. 2000). In humans, cobalt toxicity is associated with several diseases such as contact dermatitis, thyroid or neurological disorders, pneumonia, allergic asthmas and even lung cancer (Barceloux 1999).

The need for mitigation of heavy metal contamination is spurring the research for biologically based remediation technologies (bioremediation), which are considered environmental friendly (Head 1998; Hebes and Schwall 1978; Valls and de Lorenzo 2002). The understanding of the metabolic mechanisms involved in the interaction between a biological entity and a metal ion is of paramount relevance for bioremediation development, hence many efforts are being made in this direction (Guengerich 2012; Mishra and Malik 2013).

Photosynthetic organisms are ideal candidates for bioremediation, since use solar radiation as unique energy source. Among them, the photosynthetic bacterium *Rhodobacter* (*R.*) *sphaeroides* is a very interesting model, being able to adapt and grow under a wide range of environmental and nutritional conditions (Kiley and Kaplan 1988; Martinezluque et al. 1991; Schultz and Weaver 1982; Sardaro et al. 2013), as well as to tolerate and sequester metals and to reduce oxyanions (Bebien et al. 2001; Moore and Kaplan 1992; Myllykallio et al. 1999; Italiano et al. 2012). Specifically, the *R. sphaeroides* strain R26, a carotenoidless mutant highly susceptible to photooxidative stress, is able to grow in environments contaminated by high concentrations of heavy metal ions (Giotta et al. 2006; Buccolieri et al. 2006), showing a marked tolerance to cobalt ions (Italiano et al. 2009). The metabolic response of R26 mutant to cobalt stress affects the photosynthetic apparatus of the bacterium, resulting in a double effect: the down expression of porphobilinogendeaminase (PBGD), a key enzyme in the chlorophylls and heme metabolic pathway and the up-regulation of several proteins and DNA degradation enzymes, suggesting that part of the catabolic reaction products may retrieve energy and rescue bacterial growth in photosynthetically impaired cells (Italiano et al. 2007, 2008, 2011; Pisani et al. 2009; Losurdo et al. 2011).

X-ray absorption spectroscopy (XAS) is a very informative technique, which has been used in obtaining structural information on the interaction of metal ions and bacteria (Kantar et al. 2011; Boyanov et al. 2003; Mishra et al. 2009). This article investigates the fate of cobalt ions in *R. sphaeroides* R26 exposed to high Co^{2+} concentration by XAS, gaining structural insights into the cobalt coordination in three different cases, namely the whole cells, the cell envelope and the soluble portion.

Materials and methods

Sample preparation

Cells of the blue-green strain *R. sphaeroides* R26 were grown in light under anaerobic conditions by using the medium 27 of the German Collection of Microorganisms and Cell Cultures (http://www.dsmz.de), containing sub-millimolar Co^{2+} concentration. The photosynthetic growth was performed into glass vials containing the initial inoculum of the starting culture in exponential growing phase and completely filled with liquid medium, sealed, kept in the dark for 4–6 h for allowing the residual oxygen to be consumed and then exposed to light. The cultures illumination was achieved by 100 W tungsten filament light bulbs placed at 25 cm from the vessels (Buccolieri et al. 2006). Bacteria grown under these conditions are used as control samples. Cobalt effect was investigated on bacteria grown in the above medium containing a final 5 mM concentration of $CoCl_2 \times 6H_2O$ (Buccolieri et al. 2006).

XAS spectra were recorded on: (a) whole cells for control sample (WCC), (b) whole cells (WCCo), cell envelope (CECo) fraction, and soluble fraction (SCo) for cobalt exposed cells. Samples for XAS analysis were prepared as follows: one liter of cell suspension, in exponential growing phase, was centrifuged at $14{,}000 \times g$ at 4 °C for 15 min. Harvested cells from either control (WCC) or 5 mM cobalt (WCCo) conditions were washed in distilled water for at least three times and re-suspended in water. Samples CECo and SCo were obtained by adding to the washed cell, DNase I to a final 100 μg mL^{-1} and then lysed in a French pressure cell at 1.38×10^8 Pa. The resulting homogenate was centrifuged at $16{,}000 \times g$ at 4 °C for 15 min to remove

debris and unbroken cells. The supernatant was centrifuged at 150,000×*g* for 2 h to separate the cell envelope fraction from the soluble fraction.

Three standard compounds were prepared in distilled water: (i) Mod1, by direct dissolution of $CoCl_2 \times 6H_2O$ (final concentration 50 mM); (ii) Mod2, by direct dissolution of 50 mM cobalt acetate ($Co(CH_3COO)_2$); (iii) Mod3, by direct dissolution of vitamin B12 up to its saturation. Mod2 was chosen to model the cobalt ion-carboxylate compounds coordination, presumably the major interaction involved in the metal binding on the bacterial surface of *R. sphaeroides* (Giotta et al. 2011), while Mod3 was chosen as model of interaction between corrin ring and cobalt ion in B12 vitamin, the main Co-based compound in bacteria.

XAS measurements

The XAS spectra were collected on SUL-X beamline of the ANKA synchrotron at the Karlsruhe Institute of Technology. Sample solutions were mounted on aluminum holders covered by a Kapton thin foil and the measurements were performed in fluorescence mode at room temperature. Energy calibration and alignment were made with elemental cobalt foil measured in transmission and fluorescence modes. Scans were acquired at the Co–K absorption edge ($E_0 = 7{,}709$ eV), spanning the range from E = 7,500 to 8,700 eV. The XANES, pre-edge (-150 eV $< E - E_0 < -30$ eV) and near-edge regions (-30 eV $< E - E_0 < +30$ eV), were acquired with 0.25 eV energy increment. The energy step was set to 2.5 eV in the extended (EXAFS) region (up to $E - E_0 <$ +900 eV). The exposure time was about 23 min for each scan.

Possible cobalt photodegradation was tested on 5 mM $CoCl_2$, by acquiring 50 consecutive XAS spectra of 4 min each with a limited energy range (-100 eV $< E - E_0 < +200$ eV) and an energy step of 1 eV. No evidence of cobalt photodamage was detected.

Analysis of XAS spectra

XAS spectra were processed in ATHENA (Ravel and Newville 2005). Signal-to-noise ratio was improved by merging four to eight scans of the same sample. Small energy shifts between scans were corrected with the ATHENA's aligning procedure.

For the WCC control sample, XAS spectrum exhibits very low signal intensity (ten times lower than other *R. sphaeroides* samples), thus the EXAFS analysis was limited to the first shell.

For each energy value, the fluorescence intensity was divided by the X-ray beam intensity and the obtained spectra were normalized by applying a pre- and post-edge ($+300$ eV $< E - E_0 < +800$ eV) fitting procedure. Finally, the background was removed using AUTOBK algorithm (Newville et al. 1993). The normalized background-subtracted spectra, denoted as $\mu(E)$, were converted in EXAFS signals $\chi(k)$ by using the first inflection point of the absorption edge as E_0. The distributions of the radial distances from the photo-absorbing atom $|\chi(R)|$ were then obtained by applying a *k*-weighted Fourier transform to $\chi(k)$. For each sample a proper range of *k* was used to overcome the poor background removal at low *k* values (between 2.1 and 2.6 Å^{-1}) and the low signal/noise ratio at high *k* values.

Crystal structures with CCDC codes FONQUV (Zhang and Ng 2005), COAQAC01 (Sobolev et al. 2003) and GABXIS (Murtaza et al. 2010) were used as structural models for Mod1, Mod2 and Mod3, respectively (Fig. 1a–c), while the crystal structure with

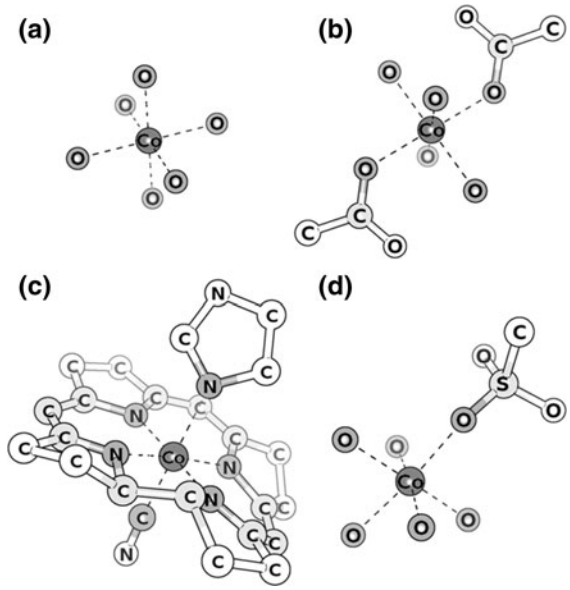

Fig. 1 Coordination shells of the structural models used for fitting EXAFS spectra: **a** hexaaquo cobalt (CCDC code FONQUV, **b** cobalt acetate (CCDC code COAQAC01), **c** B12 vitamin (GABXIS), and **d** sulfoxide-complexed cobalt, (XOHHUX)

CCDC code XOHHUX (Barton et al. 2002) was used to model the cobalt ion–sulfonic ligand interaction in *R. sphaeroides* samples (Fig. 1d). In addition, an ideal structural model containing a cobalt ion bound to six oxygen atoms (at distance of 2 Å) in octahedral coordination around the metal center was generated by using the tool "quick first-shell theory", present in the ARTEMIS (Ravel and Newville 2005), and used to calculate the contribution of multiple scattering paths in the first coordination shell.

The structural models were decomposed in terms of photoelectron scattering paths and their phase shifts, together with back-scattering amplitudes required during the fitting procedure, were calculated by FEFF 6 (Zabinsky et al. 1995). The EXAFS fitting of the normalized XAS spectra was performed by using ARTEMIS, with k^2-weighted experimental data (except Mod3, for which $k^1k^2k^3$-weight was used).

Results and discussion

Qualitative analysis of XAS spectra

The normalized, derived, and Fourier transformed spectra of each sample are shown in Fig. 2.

XANES may be conveniently used to infer the coordination symmetry of the cobalt inner-shell by using pre-edge features: the intensity of the 7.710 eV pre-edge peak, associated to the quadrupole 1s–3d transition, depends on the symmetry of the first shell and on the 3d shell occupancy extent (Jacobs et al. 2002; Juhin et al. 2010). It appears intense in tetrahedral coordination while vanishes in octahedral coordination. Distortions of these two extreme cases modify the intensity of the peak (Moen et al. 1997).

All recorded spectra show a rather small pre-edge peak at about 7.710 eV (Fig. 2a), indicating a slightly distorted octahedral first coordination shell, consisting of six light atoms (possibly oxygen and/or nitrogen). Among the observed samples, Mod3 shows a slightly higher pre-edge peak, suggesting greater distortions of the cobalt octahedral coordination symmetry for this compound, which are also evidenced by the following features: (i) all other samples show a sharp peak (Fig. 2b) in the range $-25\ \text{eV} < E - E_0 < 25\ \text{eV}$ of their μ(E) first derivative functions (Frenkel and Korshin 1999), while in Mod3 two small peaks are present, (ii) the unique 2 eV energy increase in the Co K-edge found in Mod3 points to increased charge on the cobalt center with respect to the hexaaquo coordinated ion, (iii) the radial distributions (Fig. 2c) show a peak centered around 1.6 Å for all samples excluded Mod3, where is down-shifted to 1.5 Å. This finding agrees with the shorter distances of four out of the six ligand atoms in the first shell, imposed by the presence of the corrin ring around the cobalt ion (Brink et al. 1954).

The radial distributions of Mod2, WCCo, and SCo beyond 2 Å are comparable, indicating similar second coordination shells, while significant differences emerge for Mod3, where a clear peak occurs at 2.4 Å. This Mod3 feature can be attributed to the

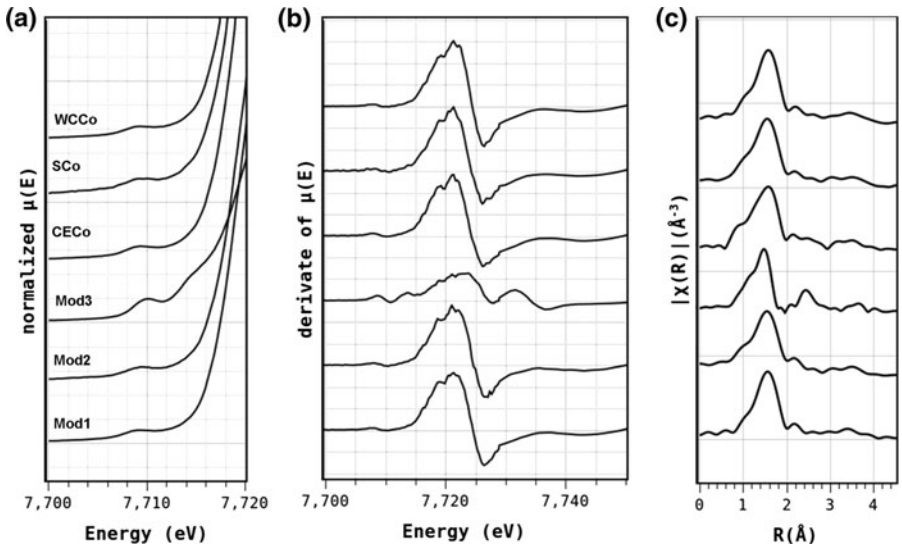

Fig. 2 Normalized μ(E) (**a**), first derivative of normalized μ(E) (**b**), and modulus of the Fourier transforms of k^2-weighted χ(*k*) (**c**) for aqueous solution of cobalt chloride (Mod1), cobalt acetate (Mod2), B12 vitamin (Mod3) and for *R. sphaeroides* samples grown in $CoCl_2$ 5 mM: cell envelope (CECo), soluble fraction (SCo), and whole cells (WCCo). Fourier transforms are shown not taking into account phase correction

complex interaction of the cobalt ion with the corrin and imidazole rings of the B12 vitamin structural model (Fig. 1c). A small specific feature at 2.6 Å may be observed in the radial distribution of CECo, indicating a different second shell coordination.

Structural analysis of model compounds

The results of the fitting procedure applied to the EXAFS signals of the model compounds are sketched in Fig. 3 in *k*- (left) and R-space (right). Good fits were obtained for all the samples, taking into account that the deviations between experimental and calculated lines occurs at *k*-values not included in the fitting range (Fig. 3, left). Multiple scattering paths between cobalt and its first-coordinating atoms were always included. This allowed to reproduce the experimental spectra beyond 3 Å and to obtain a strong improvement of statistical parameter R-factor. The estimates of structural parameters are summarized in Table 1.

Mod1 was best fitted by fixing the coordination number (CN) of the inner-shell coordinated oxygen atoms to six. Oxygen atoms are found 2.09 Å away from the cobalt, in agreement with Co–O bond distance reported for crystal of hexaaquo cobalt(II) complexes (Han et al. 2011; Wang et al. 2011; Zhang et al. 2011). The addition of multiple scattering paths halves the R-factor of the fitting (from 0.031 to 0.017).

Mod2 was fitted similarly to Mod1, obtaining a comparable Co–O bond distance (2.06 Å). The Debye–Waller factor (σ^2) of the Co–O bond is in good agreement with that found for inner-shell coordinating atoms of the cobalt/humic acids complex (Xia et al. 1997). However, the σ^2 of the two Co–C (carboxylate), in the second shell at 2.91 Å, is higher with respect to that previously obtained, suggesting greater structural disorder for Mod2 cobalt second shell. As for Mod1, the addition of multiple scattering reduces the R-factor (from 0.031 to 0.010) and two oxygen atoms were found at a distance of 4.14 Å from the cobalt ion with a Debye–Waller parameter of 0.015 $Å^2$. The large Co–O distance could be due to a carboxylate group that points only one of its two oxygen atoms towards the cobalt ion, differently from the crystal structure of cobalt acetate (Sobolev et al. 2003). Scattering contributions of these oxygen atoms and of the multiple paths allow to fully

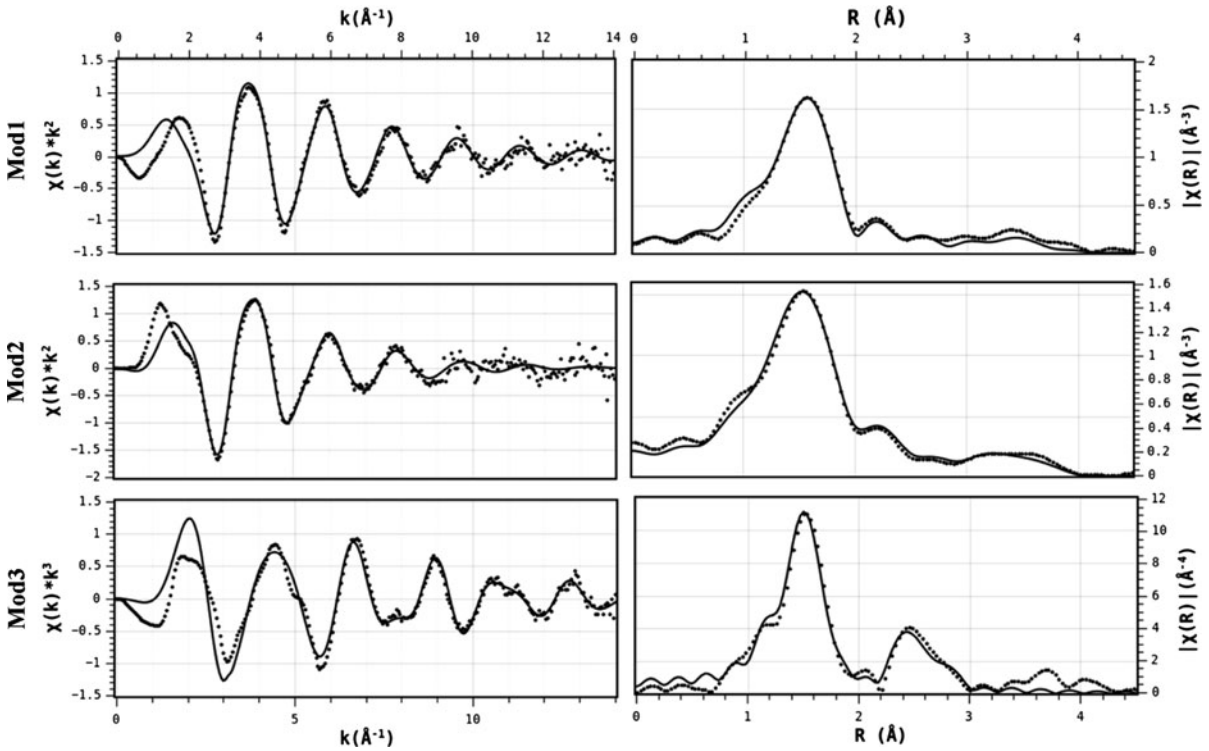

Fig. 3 Standard solutions: experimental (*dots*) and calculated (*lines*) EXAFS signals (*left*), and their respective Fourier transforms (*right*)

Table 1 Results of the EXAFS fitting procedure for standard solutions (multiple scattering paths included)

	R-factor	Global parameter		First coordination shell				Second coordination shell			
		S_0^2	E_0 (eV)	Atom	R (Å)	σ^2 (Å^2)	CN	Atom	R (Å)	σ^2 (Å^2)	CN
Mod1	0.017	0.70 (2)	7,719.2 (9)	O	2.09 (1)	0.0049 (7)	6				
Mod2	0.010	0.83 (6)	7,717.0 (9)	O	2.060 (9)	0.010 (2)	6	C	2.91 (7)	0.014*	2
Mod3	0.108	0.70*	7,722 (3)	N/C	1.900 (9)	0.0026 (7)	6	C	2.6 (1)	0.010*	2
								C	2.88 (2)	0.004 (2)*	8
								N	3.10 (6)	0.004 (5)*	1
XOHHUX[a]				O	2.08		6	S	3.41		1

Errors on the last digit are reported in brackets. Restrained parameters are marked with asterisk. No error value is reported for those that reach the limit of the restrain range. Data relative to compound XOHHUX are taken from literature

[a] Obtained from crystallographic data

Table 2 Results of the EXAFS fitting procedure for *R. sphaeroides* samples (multiple scattering paths not included)

	R-factor	Global parameter		First coordination shell				Second coordination shell			
		S_0^2	E_0 (eV)	Atom	R (Å)	σ^2 (Å^2)	CN	Atom	R (Å)	σ^2 (Å^2)	CN
CECo	0.053	0.73 (8)	7,717 (1)	O	2.08 (1)	0.006 (2)	6	S	3.30 (6)	0.013*	2
	0.053	0.71 (8)	7,717 (1)	O	2.09 (1)	0.006 (2)	6	C	2.92 (1)	0.012*	2
SCo	0.035	0.8 (1)	7,716 (1)	O	2.07 (1)	0.007 (2)	6	C	2.8 (2)	0.012*	1
WCCo	0.020	0.80 (7)	7,717 (1)	O	2.08 (1)	0.006 (1)	6	C	2.9 (1)	0.0150 (1)*	1

Errors on the last digit are reported in brackets. Restrained parameters are marked with asterisk. No error value is reported for those that reach the limit of the restrain range

reproduce the Fourier transform between 3 and 4 Å, despite a previous study on crystalline tetraaquo cobalt acetate which ascribes this feature to an artifact on the measured spectrum (Ghabbour et al. 2007).

The first shell of the cobalt ion in the Mod3 sample is also composed by six light atoms, similarly to Mod1 and Mod2, and accordingly to the B12 vitamin structure (Brink et al. 1954) contains five nitrogen (four nitrogen from the corrin ring and one from the imidazole group) and one carbon (from the cyanide group) atoms. Two carbon atoms distant 2.6 Å from the cobalt, together with other eight carbon atoms at 2.88 Å, of the corrin ring, complete the second coordination shell. In addition, a nitrogen distant 3.10 Å from the cobalt ion and belong to the imidazole ring allows a further improvement of the fit result.

Structural analysis of *R. sphaeroides* samples

EXAFS fitting result for *R. sphaeroides* samples grown in the presence of Co^{2+} are summarized in Table 2 and shown in Fig. 4 in *k*- (left) and R-space (right).

The first coordination shell of CECo sample consists of six oxygen atoms (fixed CN) with Co–O distance and Debye–Waller parameter (Table 2) comparable to Mod1 and Mod2 (Table 1). Two different second cobalt coordination shells are proposed to fit CECo: (i) two carbon atoms at 3.30 Å or (ii) two sulfur atoms at 2.92 Å can be used without significant difference of the R-factor statistical parameter. The phase shift for Co–S was obtained by using the monosulfonated complex XOHHUX (Fig. 1d). The addition of multiple scattering paths significantly reduces the R-factor in both the cases, found smaller in the Co–S case. Neither 6O–2C nor 6O–2S can fully represent the data, suggesting that the second shell can be a mixture of the two configurations. Both motifs were hence included in the fitting procedure, with the fraction of 6O–2C configuration represented by a free parameter (x). The fitting was carried out by neglecting multiple scattering paths (to avoid over fitting), fixing the structural parameters to their previously obtained best values and leaving the global parameters, E_0, S_0^2, and x free. The shell fraction containing

carbon atom was estimated as 0.494(9), leading to an R-factor of 0.051.

SCo was fitted unambiguously by using six-fixed oxygen atoms for the first shell (Fig. 4). A Co–O distance of 2.07 Å and a Debye–Waller parameter of 0.007 $Å^2$ was found, in good agreement with the structural parameters obtained from Mod1 and Mod2. The fitting improved by adding a single carbon atom in the second shell with a distance of 2.8 Å, comparable to a carbon belonging to carboxylate group binding by mono-dentate mode. (Coucouvanis et al. 1995). The Co–C path shows a Debye–Waller factor which increases up to the limit value imposed to the fitting, confirming that only one carbon atom is sufficient to explain the second shell. The addition of the multiple scattering paths strongly reduces the R-factor (from

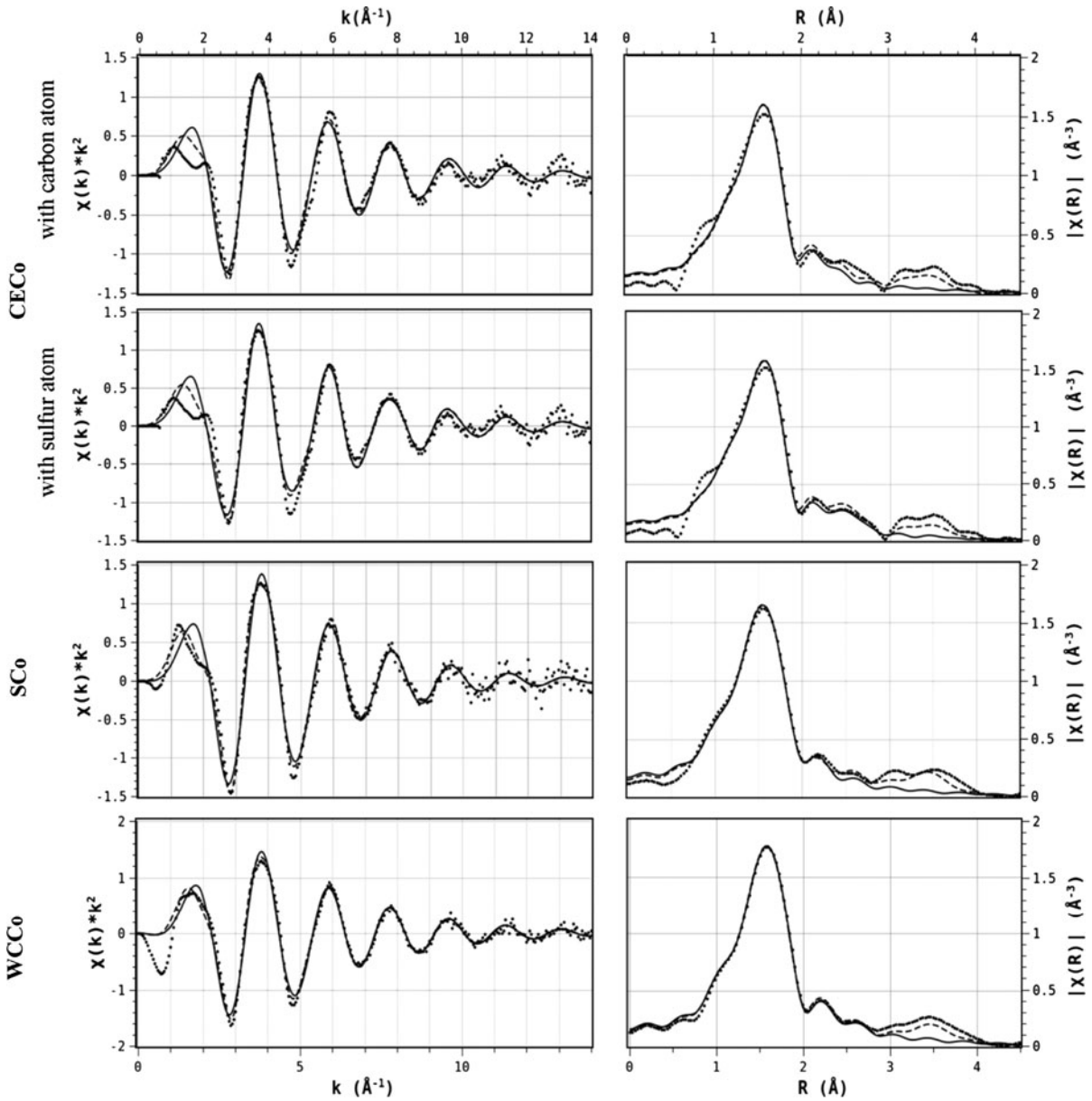

Fig. 4 *Rhodobacter sphaeroides* samples grown in 5 mM $CoCl_2$: experimental (*dots*), and calculated with (*dotted lines*) and without (*full lines*) multiple scattering paths EXAFS signals (*left*), and their respective Fourier transforms (*right*)

0.035 to 0.014), indicating a slightly-distorted octahedral coordination, in agreement with XANES and μ(E) first-derivate analysis (Fig. 2a, b). No fitting improvement was obtained by using the second oxygen atom of the carboxylate, as for Mod2.

The fitting procedure for WCCo shows first and second coordination shells similar to those in SCo (Table 2). For the second shell, the fit is also compatible with the presence of a sulfur atom at a distance of 3.2 Å, but the special fit procedure carried out by using mixed second shell structural hypotheses resulted in a value of $x > 0.95$, showing that in the soluble fraction the second shell contribution (6O–C) is the most populated one.

The EXAFS fits of the model compounds reproduce the features of the experimental patterns, up to 3 Å from the cobalt ion. For Mod1 and Mod2, the agreement was achieved up to the cobalt-center second shell. In view of this result, we carried out first and second-shell structural investigations on the *R. sphaeroides* samples containing cobalt ion. The fitting results indicate that six oxygen atoms are sufficient to explain the first strong peak of their Fourier transform (Fig. 4) with Co–O distances and Debye–Waller parameters in agreement with Mod1 and Mod2. The six-oxygen coordination explains the almost fully octahedral geometry of the cobalt coordination inferred by XANES analysis (Fig. 2a, b). The inclusion of the Co–C path was mandatory to fit the second shell of each *R. sphaeroides* sample. In all cases, the Co–C distances, obtained with no restrains, were found compatible with a mono-dentate carboxyl group, and in agreement with those obtained in cobalt ion/humic acid by Xia et al. (1997) and Ghabbour et al. (2007).

The EXAFS data of the cell-free fraction containing the cell envelope (CECo) could be fitted assuming a mixed population of the second shell, formed by a 50 % fraction of two carboxylic moieties and by a 50 % of two sulfur containing moieties. The sulfur contribution to the EXAFS data in the cell-free soluble fraction (SCo) was not detected and was found negligible in the whole cell samples (WCCo), indicating that this coordination pattern involves the cell envelope and does not appear in the soluble portion. The distance of the sulfur atom from cobalt (3.30 Å) together with the six oxygen atoms found in the first shell, indicates the presence of oxygen donor ligands having two oxygen atoms bound to a sulfur atom, as in sulfoxide or sulfonate moiety, as suggested by the structural information of compound XOHHUX.

The cell envelope of phototrophic bacteria comprises the cell wall, formed by the peptoglycane and the outer cellular membrane, and the cytoplasmic membrane (Weckesser et al. 1995), which in *R. sphaeroides* invaginates in the so-called intracytoplasmic membrane (ICM) when grown photosynthetically (Drews and Golcki 1995; D'Amici et al. 2010). The cell envelope sample CECo is a mixture of the peptoglycane, the outer membrane and cytoplasmic and intra-cytoplasmic membranes. In particular the lipid composition of cytoplasmic and intracytoplasmic membranes of *R. sphaeroides*, grown under photosynthetic conditions, consists of phosphatidylethanolamine, phosphatidylglycerol, phosphatidylcholine, cardiolipin, phosphatidic acid and sulfoquinovosyldiacyl glycerol (SQ) (Imhoff and Bias-Imhoff 1995; Fang et al. 2000; Benning et al. 1993). This latter class of lipids is characterized by a fatty acid bound to the sulfoquinovosyl, a monosaccharide containing a negatively charged sulfonate group (see Fig. 5). This membrane composition is very influenced by chemical stresses, among which the heavy metal ones (Italiano et al. 2012). The presence of a robust amount of cobalt bound to Co–O–S moiety (50 % of the total), presumably belonging to the SQ lipids, suggests that in the membrane exposed to Co^{2+}, the amount of SQ is much higher than the average 2 % found in *R. sphaeroides* under physiological condition (Benning et al. 1993). This agrees with the preliminary finding in our laboratory that in Co-exposed *R. sphaeroides* cells, sulfolipids are overexpressed.

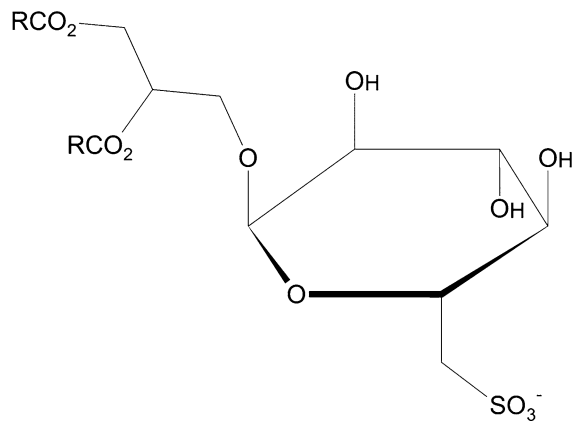

Fig. 5 Structure of the polar head of sulfolipids, the sulfoquinovosyl monosaccharide

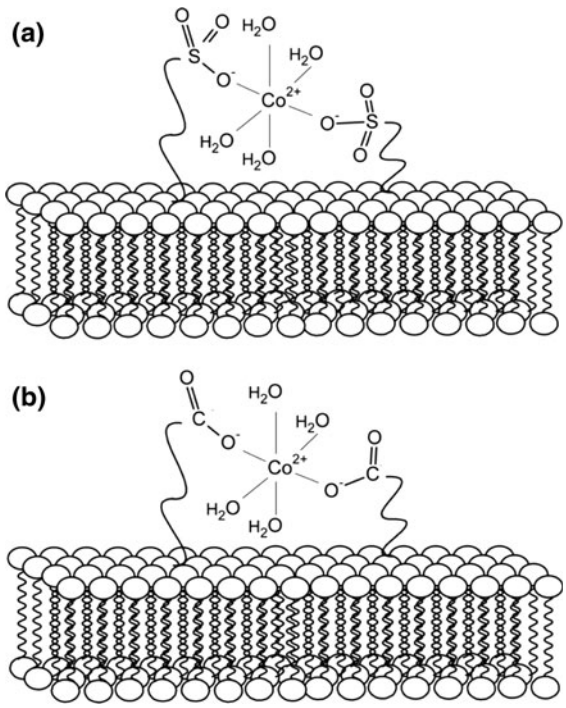

Fig. 6 Cobalt binding sites for Co. **a** Cobalt ion coordinated to four water molecules and two sulfonic groups, and **b** cobalt ion coordinated to four water molecules and two carboxylic groups

In Fig. 6 are shown two possible membrane binding sites for cobalt in the case of two OS-containing ligands (Fig. 6a) or mono-dentate carboxylate (Fig. 6b).

Differently from CECo sample, the second shell of SCo contains only a carbon atom (6O-C) evidencing that only a carboxylate group is sufficient to serve as cobalt binding site for the soluble proteome extracted from *R. sphaeroides*. In this case, the cobalt environment is made of pentaaquo ligands in addition to the mono-dentate carboxylate, excluding any other ligand in the inner-shell. Notwithstanding the different cobalt coordination for CECo and SCo samples, no mixed second shell was detected for WCCo (carboxylate fraction >95 %). This should not come as a surprise since the largest portion of a whole cells is its soluble portion, and hence the membrane represents a very small portion of the WCCo, and the Co–O–S path originating from SQ accounts for less than 5 %.

Conclusion

XAS measurements may be conveniently exploited to understand the coordination features of a metal center in a rather complex matrix such as bacterial cells. In this work, XAS was used to characterize the coordination of the cobalt ion in the presence of *R. sphaeroides*, a bacterium with high metal tolerance and considered a potential target for bioremediation process, grown in solution medium containing very high cobalt concentration. XANES measurements have shown an octahedral coordination for cobalt bound to the cell, with six oxygen atoms in the first coordination shell. EXAFS data indicates that cobalt binds to carboxylate in the soluble portion of the cell, while on the photosynthetic membrane it also binds to sulfolipids in large quantity, suggesting that this type of lipids are present in Co-exposed cells in larger quantity than control conditions, a typical response mechanism of the photosynthetic membrane of *R. sphaeroides* to abiotic stress condition.

Acknowledgments Ralph Steininger and Joerg Goettlicher at SUL-X beamline at ANKA are greatly acknowledged (Project ENV-219). Support for this work was obtained by the Italian Ministry of Research Education and Education (PRIN 2009) and by COST Action CM0902 *Molecular machinery for ion translocation across the membrane*.

References

Albering H, van Leusen S, Moonen E, Hoogewerff J, Kleinjans J (1999) Human health risk assessment: a case study involving heavy metal soil contamination after the flooding of the river Meuse during the winter of 1993–1994. Environ Health Perspect 107(1):37–43

Barceloux DG (1999) Cobalt. J Toxicol Clin Toxicol 37(2):201–206

Barton MR, Zhang Y, Atwood JD (2002) Mono-sulfonated derivatives of triphenylphosphine, $[NH_4]$TPPMS and M $(TPPMS)_2$ (TPPMS = $P(Ph)_2(m\text{-}C_6H_4SO_3^-)$; M = Mn^{2+}, Fe^{2+}, Co^{2+} and Ni^{2+}). Crystal structure determinations for $[NH_4]$TPPMS*½ H_2O, $[Fe(H_2O)_5$(TPPMS)TPPMS], $[Co(H_2O)_5$TPPMS]TPPMS and $[Ni(H_2O)_6](TPPMS)_4$*H_2O. J Coord Chem 55(8):969–983

Bebien M, Chauvin JP, Adriano JM, Grosse S, Vermeglio A (2001) Effect of selenite on growth and protein synthesis in the phototrophic bacterium *Rhodobacter sphaeroides*. Appl Environ Microbiol 67(10):4440–4447

Benning C, Beatty JT, Prince RC, Somerville CR (1993) The sulfolipid sulfoquinovosyldiacylglycerol is not required for photosynthetic electron transport in *Rhodobacter sphaeroides* but enhances growth under phosphate limitation. Proc Natl Acad Sci USA 90(4):1561–1565

Boyanov MI, Kelly SD, Kemner KM, Bunker BA, Fein JB, Fowle DA (2003) Adsorption of cadmium to *Bacillus subtilis* bacterial cell walls: a pH-dependent X-ray absorption fine structure spectroscopy study. Geochimica

et Cosmochimica Acta 67(18):3299–3311. doi: http://dx.doi.org/10.1016/S0016-7037(02)01343-1

Brink C, Hodgkin DC, Lindsey J, Pickworth J, Robertson JH, White JG (1954) Structure of vitamin B12: X-ray crystallographic evidence on the structure of vitamin B12. Nature 174(4443):1169–1171

Bruins MR, Kapil S, Oehme FW (2000) Microbial resistance to metals in the environment. Ecotoxicol Environ Saf 45(3): 198–207

Buccolieri A, Italiano F, Dell'Atti A, Buccolieri G, Giotta L, Agostiano A, Milano F, Trotta M (2006) Testing the photosynthetic bacterium *Rhodobacter sphaeroides* as heavy metal removal tool. Ann Chim 96(3–4):195–203

Coucouvanis D, Reynolds RA, Dunham WR (1995) Synthesis and characterization of a new class of asymmetric aquaacetate bridged dimers. Solid state molecular structures of the [M2(.mu.-H2O)(.mu.-OAc)2(OAc)3(Py)2]-anions (M = Mn(II), Fe(II), Co(II)). A structural model for the Fe_2 site in methane monooxygenase. J Am Chem Soc 117(28):7570–7571. doi:10.1021/ja00133a041

D'Amici GM, Rinalducci S, Murgiano L, Italiano F, Zolla L (2010) Oligomeric characterization of the photosynthetic apparatus of *Rhodobacter sphaeroides* R26.1 by nondenaturing electrophoresis methods. J Proteome Res 9(1): 192–203

Drews G, Golcki JR (1995) Structure, molecular organization and biosynthesis of membranes of purple bacteria. In: Blankenship RE, Madiga MT, Bauer CE (eds) Anoxygenic photosyntetic bacteria. Advances in photosynthesis, vol 2. Kluwer, Dordrecht, pp 231–257

Fang J, Barcelona MJ, Semrau JD (2000) Characterization of methanotrophic bacteria on the basis of intact phospholipid profiles. FEMS Microbiol Lett 189(1):67–72

Forstner U, Wittmann GTW (1983) Metal pollution in the aquatic environment. Springer, Berlin

Frenkel AI, Korshin GV (1999) A study of non-uniformity of metal binding sites in humic substances by X-ray absorption spectroscopy. Royal Society of Chemistry, Cambridge

Gault N, Sandre C, Poncy JL, Moulin C, Lefaix JL, Bresson C (2010) Cobalt toxicity: chemical and radiological combined effects on HaCaT keratinocyte cell line. Toxicol In Vitro 24(1):92–98. doi:10.1016/j.tiv.2009.08.027

Ghabbour EA, Scheinost AC, Davies G (2007) XAFS studies of cobalt(II) binding by solid peat and soil-derived humic acids and plant-derived humic acid-like substances. Chemosphere 67(2):285–291. doi:http://dx.doi.org/10.1016/j.chemosphere.2006.09.094

Giotta L, Agostiano A, Italiano F, Milano F, Trotta M (2006) Heavy metal ion influence on the photosynthetic growth of *Rhodobacter sphaeroides*. Chemosphere 62(9):1490–1499

Giotta L, Italiano F, Pisani F, Ceci LLR, De Leo F (2007) Cobalt effect on the bacteriochlorophyll biosynthesis pathway and magnesium metabolism in *Rhodobacter sphaeroides* strain R26.1. Photosynth Res 91(2–3):302–303

Giotta L, Italiano F, Buccolieri A, Agostiano A, Milano F, Trotta M (2008) Magnesium chemical rescue to cobalt-poisoned cells from *Rhodobacter sphaeroides*. In: Allen JF, Gantt E, Golbeck JH, Osmond B (eds) Photosynthesis. Energy from the sun: 14th international congress on photosynthesis, vol 1. Springer, Dordrecht, pp 1455–1458

Giotta L, Mastrogiacomo D, Italiano F, Milano F, Agostiano A, Nagy K, Valli L, Trotta M (2011) Reversible binding of metal ions onto bacterial layers revealed by protonation-induced ATR–FTIR difference spectroscopy. Langmuir 27(7):3762–3773. doi:10.1021/la104868m

Guengerich FP (2012) Thematic Minireview series: metals in biology 2012. J Biol Chem 287(17):13508–13509. doi: 10.1074/jbc.R112.355933

Han L-J, Yang S-P, Fu L–L, Gao H-L (2011) Hexaaquacobalt(II) bis(5-acetyl-2-hydroxybenzoate) dihydrate. Acta Crystallogr E 67(12):m1733. doi:10.1107/S1600536811046678

Head IM (1998) Bioremediation: towards a credible technology. Microbiology 144:599–608

Hebes SE, Schwall IR (1978) Microbial degradation of polycyclic aromatic hydrocarbons in pristine and petroleum contaminated sediments. Appl Environ Microb 35:306–316

Imhoff JF, Bias-Imhoff U (1995) Lipids, quinines and fatty acids of anoxygenic phototropic bacteria. In: Blankenship RE, Bauer CE (eds) Anoxygenic photosynthetic bacteria. Kluwer, Dordrecht, pp 179–205

Italiano F, De Leo F, Pisani F, Ceci L, Gallerani R, Zolla L, Rinalducci S, Gio L (2007) Effect of cobalt ions on the soluble proteome of *Rhodobacter sphaeroides* carotenoidless mutant. Photosynth Res 91(2–3):303

Italiano F, Pisani F, De Leo F, Ceci L, Gallerani R, Zolla L, Rinalducci S, Giotta L, Milano F, Agostiano A, Trotta M (2008) Effect of cobalt ions on the soluble proteome of a *Rhodobacter sphaeroides* carotenoidless mutant. In: Allen JF, Gantt E, Goldbeck J, Osmond B (eds) Photosynthesis. Energy from the sun: 14th international congress on photosynthesis, vol 1. Springer, Dordrecht, pp 1479–1484

Italiano F, Buccolieri A, Giotta L, Agostiano A, Valli L, Milano F, Trotta M (2009) Response of the carotenoidless mutant *Rhodobacter sphaeroides* growing cells to cobalt and nickel exposure. Int Biodeterior Biodegrad 63:948–957

Italiano F, D'Amici GM, Rinalducci S, De Leo F, Zolla L, Gallerani R, Trotta M, Ceci LR (2011) The photosynthetic membrane proteome of *Rhodobacter sphaeroides* R-26.1 exposed to cobalt. Res Microbiol 162(5):520–527

Italiano F, Rinalducci S, Agostiano A, Zolla L, De Leo F, Ceci LR, Trotta M (2012) Changes in morphology, cell wall composition and soluble proteome in *Rhodobacter sphaeroides* cells exposed to chromate. Biometals 25(5): 939–949. doi:10.1007/s10534-012-9561-7

Jacobs G, Patterson PM, Zhang Y, Das T, Li J, Davis BH (2002) Fischer–Tropsch synthesis: deactivation of noble metal-promoted Co/Al_2O_3 catalysts. Appl Catal A 233(1–2): 215–226. doi:http://dx.doi.org/10.1016/S0926-860X(02)00147-3

Jennette KW (1981) The role of metals in carcinogenesis: biochemistry and metabolism. Environ Health Perspect 40: 233–252

Juhin A, de Groot F, Vankó G, Calandra M, Brouder C (2010) Angular dependence of core hole screening in $LiCoO_2$: a DFT+U calculation of the oxygen and cobalt K-edge X-ray absorption spectra. Phys Rev B 81(11):115115

Kantar C, Demiray H, Dogan NM, Dodge CJ (2011) Role of microbial exopolymeric substances (EPS) on chromium sorption and transport in heterogeneous subsurface soils: I. Cr(III) complexation with EPS in aqueous solution.

Chemosphere 82(10):1489–1495. doi:http://dx.doi.org/10.1016/j.chemosphere.2011.01.009

Kasprzak K (1991) The role of oxidative damage in metal carcinogenicity. Chem Res Toxicol 4(6):604–615

Kiley PJ, Kaplan S (1988) Molecular genetics of photosynthetic membrane biosynthesis in *Rhodobacter sphaeroides*. Microbiol Rev 52(1):50–69

Kobayashi M, Shimizu S (1999) Cobalt proteins. Eur J Biochem 261(1):1–9

Leonard SM, Gannett P, Rojanasakul Y, Schwegler-Berry D, Castranova V, Vallyathan V, Shi X (1998) Cobalt-mediated generation of reactive oxygen species and its possible mechanism. J Inorg Biochem 70(3–4):239–244

Losurdo L, Italiano F, Trotta M, Gallerani R, Luigi RC, De Leo F (2011) Assessment of an internal reference gene in *Rhodobacter sphaeroides* grown under cobalt exposure. J Basic Microbiol 50(3):302–305

Martinezluque M, Dobao MM, Castillo F (1991) Characterization of the assimilatory and dissimilatory nitrate-reducing systems in *Rhodobacter*: a comparative-study. FEMS Microbiol Lett 83(3):329–334. doi:10.1111/j.1574-6968.1991.tb04485.x

Mishra A, Malik A (2013) Recent advances in microbial metal bioaccumulation. Crit Rev Environ Sci Technol 43(11):1162–1222. doi:10.1080/10934529.2011.627044

Mishra B, Boyanov MI, Bunker BA, Kelly SD, Kemner KM, Nerenberg R, Read-Daily BL, Fein JB (2009) An X-ray absorption spectroscopy study of Cd binding onto bacterial consortia. Geochim Cosmochim Acta 73(15):4311–4325. doi:http://dx.doi.org/10.1016/j.gca.2008.11.032

Moen A, Nicholson DG, Rnning M, Lamble GM, Lee J-F, Emerich H (1997) X-Ray absorption spectroscopic study at the cobalt K-edge on the calcination and reduction of the microporous cobalt silicoaluminophosphate catalyst Co-SAPO-34. J Chem Soc Faraday Trans 93(22):4071–4077

Moore MD, Kaplan S (1992) Identification of intrinsic high-level resistance to rare-earth oxides and oxyanions in members of the class Proteobacteria: characterization of tellurite, selenite, and rhodium sesquioxide reduction in *Rhodobacter sphaeroides*. J Bacteriol 174(5):1505–1514

Murtaza S, Ruetz M, Gruber K, Kräutler B (2010) Isovitamin B12: a vitamin B12 derivative that flips its tail. Chem Euro J 16(36):10984–10988. doi:10.1002/chem.201001616

Myllykallio H, Zannoni D, Daldal F (1999) The membrane-attached electron carrier cytochrome c(y) from *Rhodobacter sphaeroides* is functional in respiratory but not in photosynthetic electron transfer. Proc Natl Acad Sci USA 96(8):4348–4353. doi:10.1073/pnas.96.8.4348

Nevin R (2000) How lead exposure relates to temporal changes in IQ, violent crime, and unwed pregnancy. Environ Res 83(1):1–22. doi:http://dx.doi.org/10.1006/enrs.1999.4045

Newville M, Līviņš P, Yacoby Y, Rehr JJ, Stern EA (1993) Near-edge X-ray-absorption fine structure of Pb: a comparison of theory and experiment. Phys Rev B 47(21):14126–14131

Okamoto S, Eltis LD (2011) The biological occurrence and trafficking of cobalt. Metallomics 3(10):963–970. doi:10.1039/c1mt00056j

Pisani F, Italiano F, de Leo F, Gallerani R, Rinalducci S, Zolla L, Agostiano A, Ceci LR, Trotta M (2009) Soluble proteome investigation of cobalt effect on the carotenoidless mutant of *Rhodobacter sphaeroides*. J Appl Microbiol 106(1):338–349

Ravel B, Newville M (2005) ATHENA, ARTEMIS, HEPHAESTUS: data analysis for X-ray absorption spectroscopy using IFEFFIT. J Synchrotron Radiat 12(4):537–541. doi:10.1107/S0909049505012719

Sardaro A, Castagnolo M, Trotta M, Italiano F, Milano F, Cosma P, Agostiano A, Fini P (2013) Isothermal microcalorimetry of the metabolically versatile bacterium *Rhodobacter sphaeroides*. J Therm Anal Calorim 112(1):505–511. doi:10.1007/s10973-012-2895-0

Schultz JE, Weaver PF (1982) Fermentation and anaerobic respiration by *Rhodospirillum rubrum* and *Rhodopseudomonas capsulata*. J Bacteriol 149(1):181–190

Sobolev AN, Miminoshvili EB, Miminoshvili KE, Sakvarelidze TN (2003) Cobalt diacetate tetrahydrate. Acta Crystallogr E 59(10):m836–m837. doi:10.1107/S1600536803019093

Valls M, de Lorenzo V (2002) Exploiting the genetic and biochemical capacities of bacteria for the remediation of heavy metal pollution. FEMS Microbiol Rev 26(4):327–338

Wang H, Gao S, Ng SW (2011) Hexaaquacobalt(II) bis(2,2′-sulfanediyldiacetato-[kappa]3O, S, O')cobaltate(II) tetrahydrate. Acta Crystallogr E 67(11):m1521. doi:10.1107/S1600536811040979

Weckesser J, Mayer H, Schultz G (1995) Anoxygenic phototrophic bacteria: model organisms for studies on cell wall macromolecules. In: Blankenship RE, Madiga MT, Bauer CE (eds) Anoxygenic photosyntetic bacteria. Advances in photosynthesis, vol 2. Kluwer, Dordrecht, pp 207–230

Xia K, Bleam W, Helmke PA (1997) Studies of the nature of binding sites of first row transition elements bound to aquatic and soil humic substances using X-ray absorption spectroscopy. Geochim Cosmochim Acta 61(11):2223–2235. doi:http://dx.doi.org/10.1016/S0016-7037(97)00080-X

Zabinsky SI, Rehr JJ, Ankudinov A, Albers RC, Eller MJ (1995) Multiple-scattering calculations of X-ray-absorption spectra. Phys Rev B 52(4):2995–3009

Zhang X-L, Ng SW (2005) Hexaaquacobalt(II) bis(6-hydroxypyridine-3-carboxylate). Acta Crystallogr E 61(6):m1140–m1141. doi:10.1107/S1600536805014911

Zhang L-W, Gao S, Ng SW (2011) Hexaaquacobalt(II) bis[4-(pyridin-2-ylmethoxy)benzoate] dihydrate. Acta Crystallogr E 67(11):m1519. doi:10.1107/S1600536811040931